Journal of Power Sources 196 (2011) 5604–5610

Contents lists available at ScienceDirect

Journal of Power Sources

journal homepage: www.elsevier.com/locate/jpowsour

Graft copolymer-based lithium-ion battery for high-temperature operation

Qichao Hu[a,b], Sebastian Osswald[a,c], Reece Daniel[a], Yan Zhu[a,1], Steven Wesel[a,2], Luis Ortiz[a], Donald R. Sadoway[a,*]

[a] Department of Materials Science and Engineering, Massachusetts Institute of Technology, Cambridge, MA 02139, United States
[b] Department of Applied Physics, Harvard School of Engineering and Applied Sciences, Cambridge, MA 02138, United States
[c] Department of Physics, Graduate School of Engineering and Applied Science, Naval Postgraduate School, Monterey, CA 93943, United States

ARTICLE INFO

Article history:
Received 8 January 2011
Received in revised form 28 February 2011
Accepted 1 March 2011
Available online 5 March 2011

Keywords:
Graft copolymer
Polymer electrolyte
PEO
Lithium-ion battery
$LiFePO_4$
High temperature

ABSTRACT

The use of conventional lithium-ion batteries in high temperature applications (>50 °C) is currently inhibited by the high reactivity and volatility of liquid electrolytes. Solvent-free, solid-state polymer electrolytes allow for safe and stable operation of lithium-ion batteries, even at elevated temperatures. Recent advances in polymer synthesis have led to the development of novel materials that exhibit solid-like mechanical behavior while providing the ionic conductivities approaching that of liquid electrolytes. Here we report the successful charge and discharge cycling of a graft copolymer electrolyte (GCE)-based lithium-ion battery at temperatures up to 120 °C. The GCE consists of poly(oxyethylene) methacrylate-g-poly(dimethyl siloxane) (POEM-g-PDMS) doped with lithium triflate. Using electrochemical impedance spectroscopy (EIS), we analyze the temperature stability and cycling behavior of GCE-based lithium-ion batteries comprised of a $LiFePO_4$ cathode, a metallic lithium anode, and an electrolyte consisting of a 20-μm-thick layer of lithium triflate-doped POEM-g-PDMS. Our results demonstrate the great potential of GCE-based Li-ion batteries for high-temperature applications.

1. Introduction

Rechargeable lithium-ion batteries have revolutionized the consumer electronics industry and, due to their superior energy and power densities, have become the state-of-the-art energy storage technology for portable devices [1]. Applications include, but are not limited to, laptop computers, cell phones, power tools, and electrical vehicles. The use of conventional lithium-ion batteries is currently limited to near ambient temperatures (<50 °C) because of the thermal instability of electrode materials as well as the volatility and reactivity of the liquid electrolytes at elevated temperatures [1].

Conventional lithium-ion batteries comprise a lithiated transition-metal oxide cathode (e.g. $LiCoO_2$, $LiMn_2O_4$, or $LiNiO_2$), a graphite anode, poly(vinylidene fluoride) (PVDF) binder, and an electrolyte containing carbonate solvents, such as dimethyl carbonate (DMC), diethyl carbonate (DEC), ethylene carbonate (EC), or propylene carbonate (PC). Unfortunately, these solvents exhibit a poor thermal stability and high vapor pressures at elevated temperatures [2,3]. Moreover, most lithiated transition-metal oxides are known for becoming unstable in their delithiated states, particularly at high temperatures. As a consequence, in $LiCoO_2$ and $LiNiO_2$, oxygen is released from the cathode and becomes hazardous threat in the vicinity of a decomposing volatile electrolyte that is above its flash point [4–6]. While no oxygen is released below 400 °C from $LiMn_2O_4$, its delithiated state (λ-MnO_2) undergoes a phase transition at 190 °C to β-MnO_2, which is a poor lithium-ion intercalant [7,8].

Since its discovery in 1997 by Padhi et al. [9], the phospho-olivine structured $LiFePO_4$ has been a promising cathode material for lithium batteries. Upon charging, lithium ions are extracted from $LiFePO_4$ and $FePO_4$ is formed. Despite its intrinsically low electronic conductivity, which can be enhanced through either supervalent cation doping [10] or carbon coating [11–13], $LiFePO_4$ has several advantages over other cathode materials. Most importantly, $LiFePO_4$ possesses high thermal stability [4,14] and XRD studies have shown that mixtures of $LiFePO_4$ and $FePO_4$ are stable up to 300 °C [15,16]. Moreover, due to the low miscibility of $LiFePO_4$ and $FePO_4$ phases [17–19], the two-phase electrode allows for a uniquely constant discharge potential of 3.4 V relative to Li/Li^+ over a theoretical capacity of 170 mAh g^{-1} [20–22]. Finally, compared to other transition metals commonly used in lithium-ion

* Corresponding author. Tel.: +1 617 253 3487; fax: +1 617 253 5418.
E-mail address: dsadoway@mit.edu (D.R. Sadoway).
[1] Present address: Department of Physics, Massachusetts Institute of Technology, Cambridge, MA 02139, United States.
[2] Present address: Department of Chemical Engineering, Massachusetts Institute of Technology, Cambridge, MA 02139, United States.

0378-7753/$ – see front matter © 2011 Elsevier B.V. All rights reserved.
doi:10.1016/j.jpowsour.2011.03.001

battery cathodes, such as Co, V, or Mn, Fe is more earth-abundant and environmentally friendly [9].

While graphite alone exhibits high thermal stability, the carbon anodes may react with the volatile electrolytes or decomposing polymer binder at elevated temperatures. The multilayered, mosaic-structured passivation layer, often referred to as the solid-electrolyte interphase (SEI) layer protecting the graphite anode against the highly reactive electrolytes, typically undergoes decomposition at 100 °C [23]. However, the presence of a passivation film is necessary to prevent runaway corrosion of the anode by the electrolyte. Continued decomposition and re-growth of the protective layer result in the consumption of both electrolyte and anode material. This accelerates the capacity fade of the batteries and causes exothermic reactions that eventually lead to thermal runaway [24–26].

Several approaches have been explored to improve the thermal stability of rechargeable lithium-ion batteries. Novak et al. demonstrated the cycling of a Li/CuO cell with poly(ethylene oxide) (PEO) at 120 °C. However, the PEO showed low room-temperature conductivity, and the battery suffered from low operating potential and poor cyclability [27]. Ganesan et al. studied a lithium lanthanoid silicate-based solid electrolyte at temperatures up to 850 °C, but the room-temperature conductivity of the material was less than 10^{-7} S cm^{-1} [28]. Munoz-Rojas and coworkers cycled a $LiFePO_4$/Li cell at 250 °C using a molten lithium bis(trifluoromethanesulfonyl)imide (LiTFSI) salt electrolyte, but observed limited cyclability. Moreover, their battery required extensive modification to the cell construction and was not operational at temperature below the melting point of LiTFSI [29]. Recently, ionic liquids have received much attention for their thermal stability and low flammability, but their electrochemical stability at elevated temperatures remains a challenge [30].

Solid polymer electrolytes do not suffer from high volatility or high vapor pressure and exhibit higher thermal stability than do liquid electrolytes, allowing for a safe and stable operation at temperatures exceeding 100 °C. In gel or hybrid polymer electrolytes, carbonate solvents are used as plasticizers to improve the room-temperature conductivity [1] but, the volatility of these liquids limits the temperature operation window to below 90 °C.

The range of potential applications for temperature-stable lithium-ion batteries is wide. Applications may include electrical vehicles (EVs), exploration vehicles in spaceflight, and measure-while-drilling (MWD) tools used by the oil industry to mention a few. Since its first discovery in the 1970s, PEO has been the classic example of an ion-conducting polymer [31,32]. Although recent work by Zhang et al. and Gadjourova at el. demonstrated that ion conduction is possible in crystalline polymers [33,34], the majority of the previous studies focused on the amorphous phase, where ion transport is dependent on the segmental motion of the polymer chains [35–40]. When lithium salts are introduced to the polymer matrix forming PEO/LiX complexes, the oxygen atoms from both the PEO chains and the anions coordinate the lithium ions [41]. These coordination bonds are constantly formed and destroyed thus allowing for lithium-ion transport. Due to the higher chain mobility, these processes are more facile in polymers that exhibit low glass-transition temperatures (T_g). This has guided the design of polymer electrolytes, where both low T_g and suppressed crystallinity are desired to provide high ionic conductivity. At the same time, the polymer electrolyte also serves as the separator, for which mechanical integrity is a critical requirement. Therefore, a balance is needed between high conductivity, hence "liquid-like" electrical behavior, and mechanical integrity, hence "solid-like" mechanical behavior.

Trapa et al. developed an amphiphilic graft copolymer electrolyte (GCE) with a diblock structure comprising a flexible, ion-conducting poly(oxyethylene) methacrylate (POEM) block (hydrophilic) and a poly(dimethyl siloxane) (PDMS) block (hydrophobic) [42]. The chemical structure of this material is shown in Fig. 4 inset. The microphase separation between the two blocks gives rise to a mechanically stable polymer network. The low T_gs of POEM (T_g = −60 °C) and PDMS (T_g = −123 °C) confer sufficient room-temperature ionic conductivity on the material. The GCE (GC doped with the lithium salt, $LiCF_3SO_3$) has a conductivity exceeding the industry benchmark of 10^{-4} S cm^{-1} [1,26,43] at temperatures above 60 °C, and the polymer does not decompose at temperatures as high as 250–300 °C [42]. Moreover, unlike gel or plasticized polymer electrolytes, the GCE is not flammable and therefore does not constitute fire hazard, making GCE-based lithium-ion batteries a safe alternative to conventional liquid electrolyte- or gel-based cells.

While the reactivity of liquid electrolytes with elemental lithium and potential dendrite growth during charging inhibit safe operation of lithium metal anodes in conventional lithium-ion batteries, GCE-based cells have shown themselves in long-term cycle testing to be immune to these undesirable behaviors [42,63,64]. We speculate that the GCE functions as a leveling agent to prevent localized runaway deposition of lithium. Hence, switching to a solid polymer electrolyte removes the volatile components, and metallic lithium, which has almost ten times the specific capacity of graphite [44], can be safely utilized as a preferred anode material.

Here we report the high-temperature performance of polymer-based solid-state lithium-ion battery ($LiFePO_4$/GCE/Li) and demonstrate the safe operation of GCE-based cells without the need for pressure housings or other protective measures. Electrochemical impedance spectroscopy (EIS) is used to analyze the thermal stability and cycling behavior of GCE-based lithium-ion batteries comprised of a $LiFePO_4$ cathode, a metallic lithium anode, and a 20-μm-thick layer of lithium triflate-doped POEM-g-PDMS.

2. Experimental

The graft copolymer (GC) was synthesized using the robust free-radical synthesis technique described in Ref. [42]. The electrolyte was prepared by complexing lithium trifluoromethane-sulfonate or triflate ($LiCF_3SO_3$) salt (Sigma–Aldrich, 99.995% purity) into the GC at a Li:EO ratio of 1:20. Both the polymer and salt were co-solvated using tetrahydrofuran (THF) (Sigma–Aldrich, anhydrous, >99.9% purity).

In order to ensure ion conduction throughout the cathode, the GCE was also used as the binder material replacing the non-ion-conducting poly(vinylidene fluoride) (PVDF) which is commonly used in lithium batteries containing a liquid electrolyte.

The cathode was synthesized by mixing ball-milled $LiFePO_4$ powders (Linyi Gelon New Battery Materials) and carbon black (Super P), and dissolving the mixture in GCE solution at the weight ratio of 5:1:1. The resulting slurry was then sonicated, magnetically stirred to ensure proper mixing, and cast onto aluminum foil. The electrode was dried under argon atmosphere. A second layer of pure GCE solution was cast onto the dried electrode. After the solvent evaporated, the electrode was dried overnight at 80 °C inside a vacuum oven to remove the residual THF and any moisture.

Discs (area = 1.4 cm^2) were punched out of the electrode film, and assembled into CR2032 coin cells along with equal-sized metallic lithium discs (Sigma–Aldrich, 0.75 mm thick). A second set of cells comprised a commercially available $LiFePO_4$-based cathode (Valence Technology), liquid electrolyte of 1 M $LiPF_6$ in EC:DMC at 1:1 ratio (LP30, Merck), PVDF separator (Celgard), and the same metallic lithium anode (Sigma Aldrich). All cells were assembled in an argon-filled glove box with a dew point of −80 °C.

For high-temperature testing, the coin cells were wrapped in resistive heating tape, and the temperature of each cell was

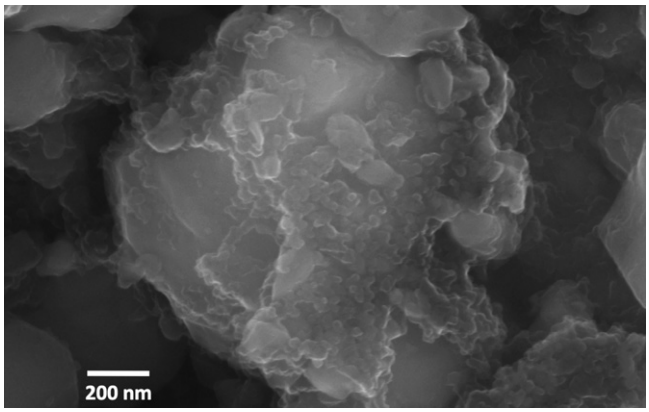

Fig. 1. SEM image of a composite cathode containing $LiFePO_4$, $LiCF_3SO_3$-doped GCE, and amorphous carbon. The $LiFePO_4$ particles are coated with both GCE and amorphous carbon allowing for high electronic and high ionic conductivities simultaneously.

measured by type-K thermocouple. In all experiments, the heating rate was less than 5 °C min^{-1}, and the temperature fluctuations remained below 2 °C. Before high-temperature measurements were performed, each cell was first cycled (3 cycles) at room temperature to form passivation layers on metallic lithium and to balance the cells.

A multichannel Maccor 4000 battery tester was used for cycle testing. EIS measurements were performed with a Solartron Electrochemical Interface 1286 coupled to a Solartron Frequency Response Analyzer 1260. Scans ranged from 1 MHz to 100 mHz under an AC potential of 10 mV at open circuit. The software Zsim (EChem Software) was used to fit the data and to generate impedance plots. Scanning electron microscopy (SEM) images were made with a Zeiss Supra using an electron beam of 27 kV and magnification of 70k×. Fourier transform infrared spectroscopy (FTIR) was performed with a Thermo Nicolet NEXUS 670 spectrometer equipped with a diamond attenuated total reflection (ATR) accessory. ATR-IR spectra were obtained at 1 cm^{-1} resolution and summed over 100 scans. Isothermal thermogravimetric analysis (TGA) was done under flowing nitrogen using a TA Instruments Q50. Differential scanning calorimetry (DSC) was performed using a Q1000 differential scanning calorimeter (TA Instruments). The heating/cooling rate was 10 °C min^{-1}, and the nitrogen purge rate was 50 mL min^{-1}.

3. Results and discussion

Fig. 1 shows the SEM image of a composite cathode comprised of $LiFePO_4$, $LiCF_3SO_3$-doped GCE, and amorphous carbon. Using the slurry casting technique, $LiFePO_4$ particles were coated with both amorphous carbon and GCE thus providing both electronic and ionic conduction paths throughout the entire electrode.

The room-temperature charge and discharge characteristics of a $LiFePO_4$/GCE/Li battery are shown in Fig. 2a in comparison to those of a conventional $LiFePO_4$/LP30/Li cell. While the GCE-based cells exhibit a slightly larger overpotential than their liquid

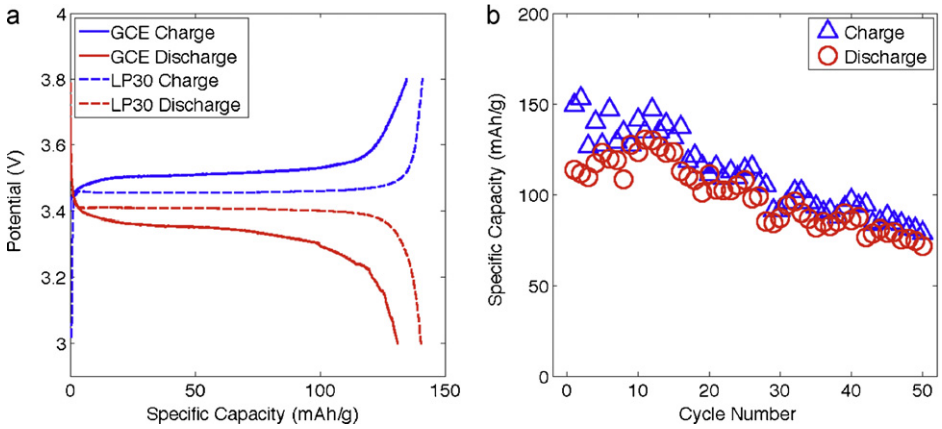

Fig. 2. Room-temperature charge and discharge curves of $LiFePO_4$/GCE/Li and commercial $LiFePO_4$/LP30/Li cells (a), and capacity changes of the $LiFePO_4$/GCE/Li battery during cycle-testing (b). The current densities used in these experiments were 10 mA g^{-1} and 15 mA g^{-1} for $LiFePO_4$/GCE/Li and commercial $LiFePO_4$/LP30/Li, respectively.

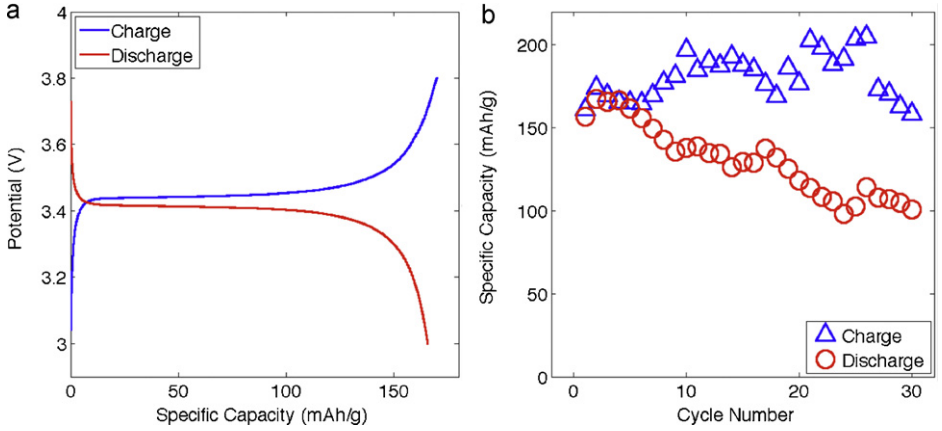

Fig. 3. Charge and discharge curves (a) and cycling capacity (b) of $LiFePO_4$/GCE/Li at 120 °C. The current density used was 10 mA g^{-1}.

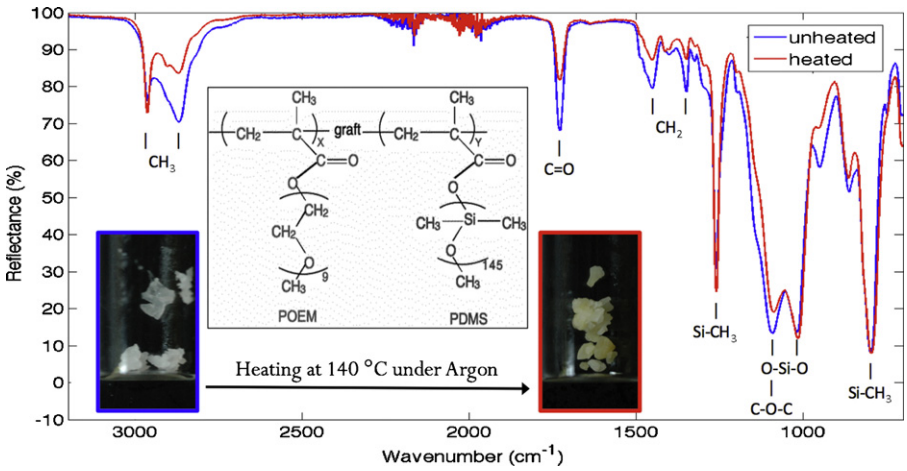

Fig. 4. FTIR spectra of unheated and heated (140 °C) graft copolymer. Chemical structure of the graft copolymer (inset). The graft copolymer shows discoloration after heating (inset).

electrolyte-based counterparts, the discharge capacity is similar to that of LP30-based Li-ion batteries (~150 mAh g^{-1}). The theoretical specific capacity of $LiFePO_4$ (~170 mAh g^{-1}) is not achieved since it is limited by the lithium diffusion within $LiFePO_4$ particles, which is low at room temperature [45,46]. Upon room-temperature cycling (Fig. 2b) the discharge capacity of the $LiFePO_4$/GCE/Li cell increases during the first 10–15 cycles, followed by a slight capacity fade (~1.1% per cycle). The energy efficiency during the first few cycles is low (large charge/discharge capacity ratio), possibly due to the irreversible capacity loss related to the formation of the passivation layer at lithium anode. The passivation film could result from reactions between lithium and residual THF solvent or the $CF_3SO_3^-$ anions, which are known to produce LiF species [47].

High-temperature testing of the $LiFePO_4$/GCE/Li cells (Fig. 3a) showed that the charge/discharge performance at 120 °C (Fig. 3a) is comparable to that of the commercial $LiFePO_4$/LP30/Li cells at room temperature (compare Figs. 2a and 3a). Moreover, due to the increased Li-ion mobility in $LiFePO_4/FePO_4$ mixed phases at elevated temperature, nearly the full theoretical specific capacity of 170 mAh g^{-1} is achieved [48]. Fig. 3b shows charge/discharge capacity of $LiFePO_4$/GCE/Li cells upon cycling at 120 °C with a capacity retention exceeding 100 mAh g^{-1} for 30 cycles.

We observed a decreasing energy efficiency after the first few cycles due to an increasing charge capacity and steady fade in discharge capacity, consistent with the results reported by Andersson el al. [46]. Since the charge capacity of $LiFePO_4$ cannot exceed ~170 mAh g^{-1}, the excessive capacity must be ascribed to other electron consuming reactions, such as the formation of a passivation layer. Temperature-induced volume expansion of metallic lithium may exert mechanical stress on the passivation film, leading to cracking and the exposure of fresh lithium to the electrolyte.

Isothermal TGA study of the GC at 140 °C under inert atmosphere revealed a weight loss of less than 2% over 50 h. However, the graft copolymer showed discoloration after long exposure to elevated temperatures (Fig. 4 inset). FTIR analysis of the GC before and after heating revealed cleavage of different bonds within the polymer (Fig. 4). The most significant changes upon heating are the decreases in the symmetric and asymmetric stretching modes of C–H in the methyl CH_3 (peaks between 2800 and 3000 cm^{-1}) and the stretching mode of the carbonyl (C=O) groups (~1730 cm^{-1}),

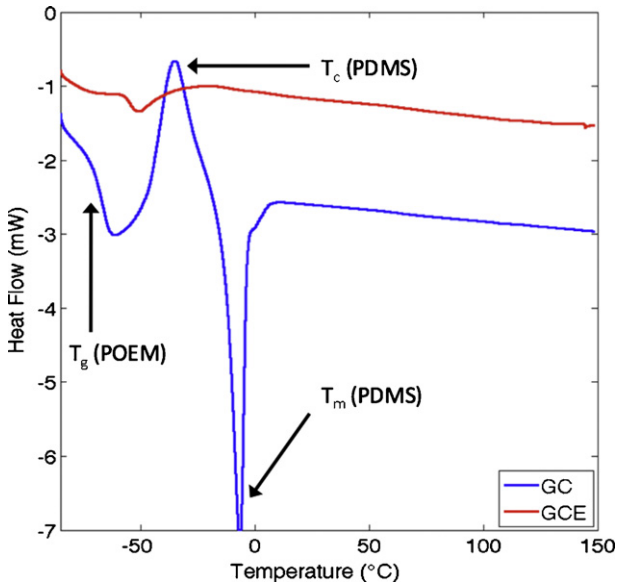

Fig. 5. DSC spectra of undoped graft copolymer (GC) and doped graft copolymer electrolyte (GCE). The cooling and heating rates were 10 °C min^{-1}.

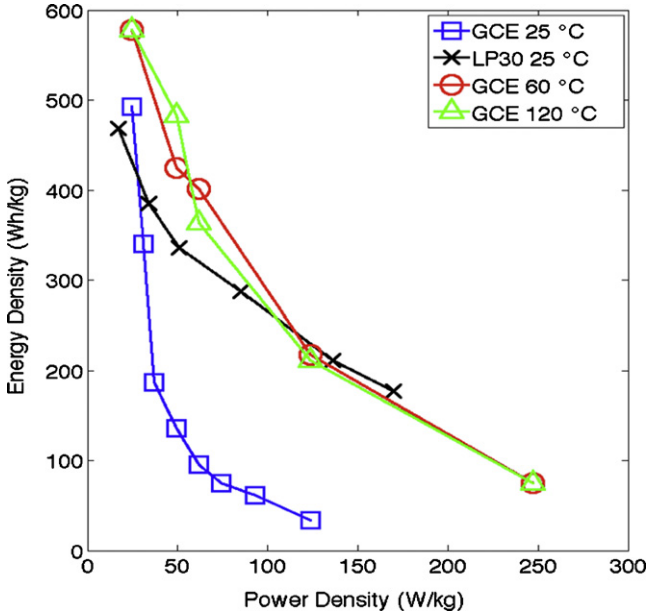

Fig. 6. Ragone plot for $LiFePO_4$/GCE/Li cells at various temperatures in comparison to room-temperature measurements obtained from $LiFePO_4$/LP30/Li battery.

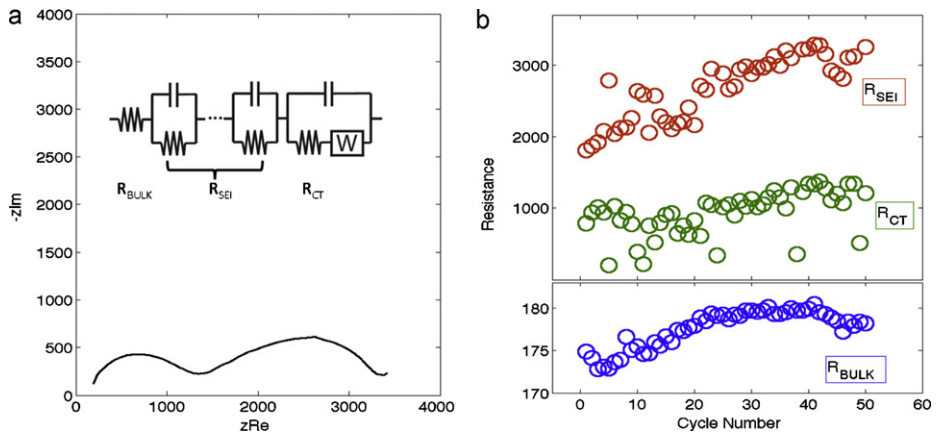

Fig. 7. Typical EIS spectrum for $LiFePO_4$/GCE/Li (a) and equivalent circuit model (a inset). Evolution of various impedance components during room-temperature cycling (b).

both of which are associated with the methacrylate backbone. Decays are also observed in O–Si–O (from the PDMS sidechain), C–O–C, and C–H in CH_2 (from the POEM sidechain). Si–CH_3 remains stable during heating [49–51].

Despite the potential bond cleavages in the PDMS domain and the backbone after prolonged heating, both the undoped graft copolymer (GC) and the doped graft copolymer electrolyte (GCE) are stable and do not undergo additional phase transformations or decomposition reactions above 60 °C, as evident in the DSC heating curves shown in Fig. 5. In the case of GC, the T_g of the POEM domain is observed at approximately −67 °C. The exothermic peak around −35 °C is associated with the crystallization temperature (T_c) of the PDMS domain, while the endothermic peak around −7 °C corresponds to the melting temperatures (T_m) of the PDMS domain [42,52]. In the lithium triflate-doped GCE curve, no T_c or T_m from the PDMS domain is observed, while the T_g of the POEM domain is observed at −55 °C. The higher T_g in the POEM domain and the absence of T_m and T_c in the PDMS domain of the GCE suggest that the solvation of the Li^+ cations by the PEO units reduces the segmental motion in the amorphous POEM domain and suppresses the crystallinity in the PDMS domain. In both cases no crystallization or melting of the POEM domain is observed, suggesting that PEO is completely amorphous.

So far, for both low-temperature (Fig. 2) and high-temperature (Fig. 3) charge and discharge cycling, relatively low current densities (<15 mA g^{-1}) were used. Fig. 6 shows the Ragone plot for the GCE cells at various temperatures, reflecting the tradeoff between energy density and power density. At large currents, the cell performance becomes diffusion-limited and the cell capacity decreases. For the LP30-based cells, only room-temperature data were recorded. In the case of the GCE-based cells, performance at ∼60 °C is of particular interest since this temperature is in the range of the melting point of PEO [43,53,54]. As indicated in Fig. 6, at room temperature the energy densities of the GCE and LP30-based cells are comparable at low power densities. As the power density is increased from 25 to 50 W kg^{-1}, the energy density of the GCE-based cell falls drastically. However, at elevated temperatures (>60 °C), the decrease in energy density of the GCE-based cell with increasing power density is significantly smaller due to the higher mobility of PEO chains. Above 60 °C, the performance of the GCE-based cell becomes less dependent on temperature and comparable to the room-temperature performance of the liquid electrolyte-based cells.

EIS was used to study changes in resistance of the various cell components and to evaluate their dependence on cycling and temperature. Fig. 7a shows the Nyquist plot of a fully discharged $LiFePO_4$/GCE/Li cell and the corresponding equivalent circuit model (ECM) used for EIS analysis (inset in Fig. 7a) [55–57]. At high frequency, a non-zero x-axis intercept indicates the presence of solution resistance, or resistance through the bulk GCE (R_{BULK}) [42], and is represented by a resistor in the ECM. In the high frequency region, several overlapping semicircles associated with lithium-ion transport through a multilayered passivation film are observed (R_{SEI}). The multilayer characteristic of the passivation film is represented by multiple R‖C parallel circuits in series, akin to the Voight model [58]. At medium and low frequencies, the impedance contributions result primarily from the charge-transfer resistance (R_{CT}) and double-layer capacitance (C_{DL}) at the electrode/electrolyte

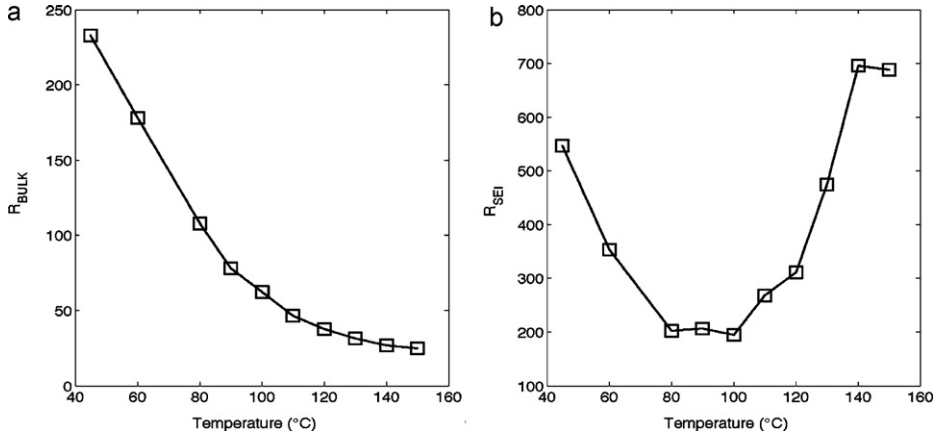

Fig. 8. Impedance through bulk electrolyte (a) and across interfacial layers (b) as function of increasing temperature.

interface, as well as solid-state diffusion through the active electrode materials (Warburg element) [59,60].

In order to analyze changes in the impedance of $LiFePO_4$/GCE/Li cells upon cycling, EIS was performed after each cycle (fully discharged state) for 50 cycles at room temperature, and the parameters extracted from the fitting program are plotted in Fig. 7b. We observe that R_{BULK} increases in the early cycles but quickly stabilizes, suggesting no or littler changes in the GCE during long cycling. Similarly, R_{CT} remains relatively constant upon cycling, revealing a high thermal stability of the electrode materials. In the case of R_{SEI}, 5 $R\|C$ elements were used to fit the interfacial passivation film and the sum of their resistances is plotted. A total of 14 circuit elements was used in the fitting. We observe a steady increase in R_{SEI}, indicating an unimpeded growth of the SEI layer, and causing the capacity fade seen in Fig. 2b. As illustrated in Fig. 7b, the overall cell resistance is dominated by R_{SEI} and R_{CT}, suggesting that the performance-limiting factor is not the electrolyte but the electrode/electrolyte interface. Future work on lithium polymer batteries should therefore focus not only on optimizing the conductivity of the polymer electrolyte, but also on modifying the electrode/electrolyte interface to decrease interfacial impedance.

In Fig. 8, EIS is performed on discharged $LiFePO_4$/GCE/Li cells after the 5th cycle at various temperatures. Since R_{BULK} (Fig. 8a) is simply the resistance of the pure GCE, its temperature dependence agrees with the Vogel–Fulcher–Tammann behavior typical for polymer conduction in the amorphous phase [42]. However, the interfacial impedance, R_{SEI} (Fig. 7b), goes through a minimum, decreasing up to 80 °C and then increasing above 100 °C. This is consistent with changes in the reaction selectivity in the passivation film, causing the film to be more resistant to lithium transport, and leading to discharge capacity fade seen in Fig. 3b.

4. Conclusion

In this study, we show for the first time that Li-ion batteries can safely be operated over a wide temperature range, reaching temperatures up to 120 °C or more, without the need of pressure housing or other protective measures. Since both the cathode and the GC are shown to be stable up to 300 °C, it is most likely the anode that dictates the current temperature limitations. Indeed, at higher temperatures (>120 °C) metallic lithium becomes too reactive, leading to the observed capacity fade. Switching to a more temperature-stable anode, such as graphite or a lithium alloy, may further increase the upper temperature limit of operation. However, a trade-off between energy density, cycle life, and temperature stability must be made since these alternative anode materials each exhibit lower capacities and/or experience significant volume changes that limit the cycle life [61].

The physical model of lithium polymer batteries is complicated by the presence of an interfacial passivation film, not to mention by diffusion and transport processes within the bulk electrolyte and electrodes [62]. While EIS can be used to differentiate between the various components, future studies using in situ Raman spectroscopy, FTIR, and electron microscopy techniques will be required to identify the molecular species involved, and to validate the assumptions made from EIS data. Both room and elevated temperature EIS data presented in this study indicate that the dominant performance-limiting factor in a cell fitted with a GCE is not associated with the electrolyte or the electrodes, but with the electrode/electrolyte interfaces. Understanding these interfacial phenomena will be key to the development of safe, polymer-based solid-state lithium-ion batteries.

Acknowledgments

This work was supported in part by Chevron. Qichao Hu would also like to thank the Harvard Graduate Consortium on Energy and Environment for its fellowship.

References

[1] J.-M. Tarascon, M. Armand, Nature 414 (2001) 359–367.
[2] N. Takami, M. Sekino, T. Ohsaki, M. Kanda, M. Yamamoto, Journal of Power Sources 97–98 (2001) 677–680.
[3] B. Ravdel, K.M. Abraham, R. Gitzendanner, J. DiCarlo, B. Lucht, C. Campion, Journal of Power Sources 119–121 (2003) 805–810.
[4] J.R. Dahn, E.W. Fuller, Solid State Ionics 69 (1994) 265–270.
[5] Y. Baba, S. Okada, J.-I. Yamaki, Solid State Ionics 148 (2002) 311–316.
[6] J. Yamaki, Y. Baba, N. Katayama, H. Takatsuji, M. Egashira, S. Okada, Journal of Power Sources 119–121 (2003) 789–793.
[7] M.M. Thackeray, A.D. Kock, L.A.D. Picciotto, Journal of Power Sources 26 (1989) 355–363.
[8] J.M. Tarascon, D. Guyomard, Electrochimica Acta 38 (1993) 1221–1231.
[9] A.K. Padhi, K.S. Nanjundaswamy, J.B. Goodenough, Journal of Electrochemical Society 144 (1997) 1188–1194.
[10] S.-Y. Chung, J.T. Bloking, Y.-M. Chiang, Nature Materials 1 (2001) 123–128.
[11] H. Huang, S.-C. Yin, L.F. Nazar, Electrochemical and Solid-State Letters 4 (2001) A170–A172.
[12] P.P. Prosini, D. Zane, M. Pasquali, Electrochimica Acta 46 (2001) 3517–3523.
[13] N. Ravet, Y. Chouinard, J.F. Magnan, S. Besner, M. Gauthier, M. Armand, Journal of Power Sources 97 (2001) 503–507.
[14] M. Takahashi, Journal of the Electrochemical Society 152 (2005) A899–A904.
[15] M. Koltypin, D. Aurbach, L. Nazar, B. Ellis, Journal of Power Sources 174 (2007) 1241–1250.
[16] M. Koltypin, D. Aurbach, L. Nazar, B. Ellis, Electrochemical and Solid-State Letters 10 (2007) A40–A44.
[17] B.L. Ellis, W.R.M. Makahnouk, Y. Makimura, K. Toghill, L.F. Nazar, Nature Materials 6 (2007) 749–752.
[18] B. Ellis, L.K. Perry, D.H. Ryan, L.F. Nazar, Journal of American Chemical Society 128 (2006) 11416–11422.
[19] A. Yamada, H. Koizumi, S. Nishimura, N. Sonoyama, R. Kanno, M. Yonemura, T. Nakamura, Y. Kobayashi, Nature Materials 5 (2006) 357–360.
[20] C. Delacourt, P. Poizot, J.-M. Tarascon, C. Masquelier, Nature Materials 4 (2005) 254.
[21] C. Delmas, M. Maccario, L. Croguennec, F.L. Cras, F. Weill, Nature Materials 7 (2008) 665.
[22] P. Gibot, M. Casas-Cabanas, L. Laffont, S. Levasseur, P. Carlach, S. Hamelet, J.-M. Tarascon, C. Masquelier, Nature Materials 7 (2008) 741.
[23] F. Kong, R. Kostecki, G. Nadeau, X. Song, K. Zaghib, K. Kinoshita, F. McLarnon, Journal of Power Sources 97–98 (2001) 58–66.
[24] D. Aurbach, M.L. Daroux, P.W. Faguy, E. Yeager, Journal of Electrochemical Society 134 (1987) 1611–1620.
[25] D. Aurbach, B. Markovsky, M.D. Levi, E. Levi, A. Schechter, M. Moshkovich, Y. Cohen, Journal of Power Sources 81–82 (1999) 95–111.
[26] J.B. Goodenough, Y. Kim, Chemical Materials 22 (2010) 587–603.
[27] P. Novak, P. Podhajecky, Journal of Power Sources 35 (1991) 235–247.
[28] M. Ganesan, Electrochemistry Communications 9 (2007) 1980–1984.
[29] D. Munoz-Rojas, J.-B. Leriche, C. Delacourt, P. Poizot, M. Palacin, J.-M. Tarascon, Electrochemistry Communications 9 (2007) 708–712.
[30] J. Mun, Y. Jung, T. Yim, H. Lee, H. Kim, Y. Kim, S. Oh, Journal of Power Sources 194 (2009) 1068–1074.
[31] D.E. Fenton, Polymer 14 (1973) 589.
[32] M.B. Armand, Fast Ion Transport in Solids (1979) 131.
[33] Z. Gadjourova, Y.G. Andreev, D.P. Tunstall, P.G. Bruce, Nature 412 (2001) 520–523.
[34] C. Zhang, S. Gamble, D. Ainsworth, A.M.Z. Slawin, Y.G. Andreev, P.G. Bruce, Nature Materials 8 (2009) 580–584.
[35] J.B. Kerr, S.E. Sloop, G. Liu, Y.B. Han, J. Hou, S. Wang, Journal of Power Sources 110 (2002) 389–400.
[36] J. Hassoun, P. Reale, B. Scrosati, Journal of Materials Chemistry 17 (2007) 3668–3677.
[37] G.B. Appetecchi, W. Henderson, P. Villano, M. Berrettoni, S. Passerini, Journal of the Electrochemical Society 148 (2001) A1171–A1178.
[38] F. Croce, G.B. Appetecchi, L. Persi, B. Scrosati, Nature 394 (1998) 456–458.
[39] F. Croce, R. Curini, A. Martinelli, L. Persi, F. Ronci, B. Scrosati, Journal of Physical Chemistry B 103 (1999) 10632–10638.
[40] G. Mao, R.F. Perea, W.S. Howells, D.L. Price, M.-L. Saboungi, Nature 405 (2000) 163–165.
[41] P. Lightfoot, M.A. Mehta, P.G. Bruce, Science 262 (1993) 883–885.
[42] P.E. Trapa, Y.-Y. Won, S.C. Mui, E.A. Olivetti, B. Huang, D.R. Sadoway, A.M. Mayes, S. Dallekb, Journal of the Electrochemical Society 152 (2005) A1–A5.
[43] R.C. Agrawal, G.P. Pandey, Journal of Physics D: Applied Physics 41 (2008) 1–18.
[44] A.S. Arico, P. Bruce, B. Scrosati, J.-M. Tarascon, W.V. Schalkwijk, Nature Materials 4 (2005) 366–377.
[45] M. Takahashi, S. Tobishima, K. Takei, Y. Sakurai, Journal of Power Sources 97–98 (2001) 508–511.

[46] A.S. Andersson, J.O. Thomas, B. Kalska, L. Häggström, Electrochemical and Solid-State Letters 3 (2000) 66–68.
[47] E. Peled, O. Golodnitsky, G. Ardel, Journal of the Electrochemical Society 144 (1997) L208–L210.
[48] C. Delacourt, P. Poizot, J.-M. Tarascon, C. Masquelier, Nature Materials 4 (2005) 254–260.
[49] J.H. Koh, K.J. Lee, J.A. Seo, J.H. Kim, Journal of Polymer Science: Part B: Polymer Physics 47 (2009) 1443–1451.
[50] B. Yang, C. Guo, S. Chen, J. Ma, J. Wang, X. Liang, L. Zheng, H. Liu, Journal of Physical Chemistry 110 (2006) 23068–23074.
[51] J. Zhou, H. Yan, K. Ren, W. Dai, H. Wu, Analytical Chemistry 81 (2009) 6627–6632.
[52] T. Dollase, H.W. Spiess, M. Gottlieb, R. Yerushalmi-Rozen, Europhysics Letters 60 (2002) 390–396.
[53] J.B. Kerr, G. Liu, L.A. Curtiss, P.C. Redfern, Electrochimica Acta 48 (2003) 2305–2309.
[54] O. Buriez, Y.B. Han, J. Hou, J.B. Kerr, J. Qiao, S.E. Sloop, M. Tian, S. Wang, Journal of Power Sources 89 (2000) 149–155.
[55] P.L. Moss, G. Au, E.J. Plichta, J.P. Zheng, Journal of Power Sources 189 (2009) 66–71.
[56] P.L. Moss, G. Au, E.J. Plichta, J.P. Zheng, Journal of the Electrochemical Society 157 (2010) A1–A7.
[57] M.D. Levi, D. Aurbach, Journal of Physical Chemistry B 101 (1997) 4630–4640.
[58] P. Agarwal, M.E. Orazem, Journal of the Electrochemical Society 139 (1992) 1917.
[59] D. Aurbach, A. Zaban, Journal of Electroanalytical Chemistry 348 (1993) 155.
[60] D. Aurbach, A. Zaban, Journal of Electroanalytical Chemistry 367 (1994) 15.
[61] Y. Idota, T. Kubota, A. Matsufuji, Y. Maekawa, T. Miyasaka, Science 276 (1997) 1395–1397.
[62] J.-M. Atebamba, J. Moskon, S. Pejovnik, M. Gaberscek, Journal of the Electrochemical Society 157 (2010) A1218.
[63] D.R. Sadoway, A.M. Mayes, B. Huang, S. Mui, P.P. Soo, D.H. Staelin, C.C. Cook, Journal of Power Sources 97–98 (2001) 674–676.
[64] P.E. Trapa, B. Huang, D.R. Sadoway, A.M. Mayes, Electrochemical and Solid-State Letters 5 (5) (2002) A85–A88.